WPMAT-PR(18) 19249

MJ Caturla et al.

Object kinetic Monte Carlo methods applied to modeling radiation effects in materials

Preprint of Paper to be submitted for publication in
Computational Materials Science

This work has been carried out within the framework of the EUROfusion Consortium and has received funding from the Euratom research and training programme 2014-2018 under grant agreement No 633053. The views and opinions expressed herein do not necessarily reflect those of the European Commission.

Object kinetic Monte Carlo methods applied to modeling radiation effects in materials

María J. Caturla*
Dept. Física Aplicada, Facultad de Ciencias, Fase II, Universidad de Alicante, E-03690, Spain

Abstract

The object kinetic Monte Carlo method has proven to be an excellent tool to better understand microstructure evolution in irradiated materials, from metals to semiconductors. Its most valuable capability is that it provides a way to connect those parameters obtained from fundamental models, such as first principles calculations, to experimental observations by expanding the time and length scales. However, this method has many limitations that pose questions on its predictive capabilities, therefore an important effort is taking place to improve the model. In this review, firstly the methodology of object kinetic Monte Carlo is described, a few examples are then presented in the field of radiation damage of metals and finally the limitations of the method and its applicability is discussed. To conclude, an outlook on the future of this computational model is given.

Keywords: Kinetic Monte Carlo, radiation damage, metals

* E-mail address: mj.caturla@ua.es

1. Introduction

Irradiation of materials can result in defects that alter their mechanical, electrical, thermal and/or magnetic properties. In some cases, irradiation is the means to tailor the properties, as in the case of ion implantation of semiconductors [1]. In other cases, defects are an unavoidable effect that act in detriment of the material properties, as in the case of systems exposed to high radiation levels in nuclear reactors [2, 3]. With the advance of nanotechnology, focused ion beams are used to fabricate nanoscale features [4] and questions still remain as to the effect of the radiation damage produced by this technique [5]. Understanding the phenomena behind defect production and defect evolution is key in all these different applications, either to select the most appropriate material, such as in the case of nuclear applications, or to improve the technique, as in ion implantation of semiconductors or focused ion beams.

In fact, all these different applications and experimental conditions have something in common: defects are produced in a time scale of picoseconds and are atomic scale in size, giving rise to out-of-equilibrium phenomena that can evolve over much longer time and length scales until reaching a steady-state. This is, therefore, a complex phenomena that can not be tackled by a single simulation model, and a multiscale approach must be used [6]. The initial damage produced by the energetic particles within the picosecond time scale can be modeled using binary collision approximation methods together with molecular dynamics simulations with empirical potentials, as explained in sections 4 and 5 of this special issue. The number of defects produced as well as their spatial distribution and configuration can be obtained from these calculations and this information is crucial for the subsequent microstructure evolution, as we will show in a few examples in this review.

Object kinetic Monte Carlo (OKMC) is able to extend the time and length scale of molecular dynamics simulations to times and sizes that are comparable to experimental observations. For example, the average time between two ions during ion implantation is on the order of miliseconds. The migration energy of a self-interstitial in Fe according to density functional theory calculations is ~ 0.3 eV [7]. Therefore, many processes can occur in between cascades, that can not be captured using molecular dynamics alone, since time scales on the order of miliseconds are not accessible. This is where OKMC can be a very useful tool. Unlike molecular dynamics simulations, in OKMC the vibrations of each atom around its equilibrium position is not modeled, and only the rare events are followed. However, this also implies that the relevant events to be included in the model have to be selected. And there is no unambiguous method to select these processes; it is to the discretion of the modeler to decide which processes are those that must be included. This is one of the limitations of this technique. Once all the probabilities of all the possible events are known, the algorithm evolves the system according to these probabilities until the final conditions are met, either total simulated time or total irradiation dose. These results can be directly compared to experimental observations such as transmission electron microscopy (TEM), positron annihilation experiments (PAS), small angle neutron scattering (SANS) or atom probe tomography (APT), methods that can provide information about defect concentration with dose, defect sizes and character. Contrasting the results of the calculations with different experimental observations is necessary to verify the reliability of the model considered.

In the following we will describe the OKMC algorithm, and briefly two related Monte Carlo methods, the so-called event kinetic Monte Carlo and the first-passage kinetic Monte Carlo. Several examples are presented, focused on the influence of the initial damage distribution

obtained from molecular dynamics with empirical potentials on the microstructure evolution in the case of irradiated metals.

2. Methodology

Monte Carlo models are those where the main algorithm is based on a stochastic component. Consequently, there is a wide variety of algorithms under the name Monte Carlo and used for very different applications from materials modelling to risk assessment in finance [8]. The first Monte Carlo method is attributed to Ulam and Metropolis, developed while working at the Los Alamos National Laboratory during the Manhattan project [9]. See references [10, 11] for the history of this development. In the field of defects, the first simulations were done a few years later by Beeler [12], followed by those of Besco [13] and Doran [14] applied to study short-term annealing of defects in f.c.c. and b.c.c. materials.

The kinetic Monte Carlo (KMC) method that will be discussed here follows the kinetics of a series of events with known probabilities of occurrence. It was first used in the field of radiation damage by H. Heinisch in the early 90's [15] and since then it has been applied to different metals, particularly iron and iron alloys [7, 16-19] and tungsten [20, 21], to name a few. In the case of radiation effects the events are related to migration of defects, dissociation of defect clusters or interaction between different types of defects among themselves or with the existing microstructure. These are slow processes or rare events that can not be followed with methods like molecular dynamics, where time scales of only a few nanoseconds can be achieved, as mentioned above. In KMC, once all the different types events and event rates are known, the system evolves according to those rates, and different algorithms can be used for this time evolution. One such algorithms is the so-call residence time or Bortz-Kalos-Liebowitz (BKL) [22]. When this approach is used, the KMC algorithm is often called Object kinetic Monte Carlo (OKMC). Here, the total rate for all possible events is calculated as:

$$R = \sum_{i=1}^{e} \Gamma_i N_i \quad (1)$$

where *e* is the total number of possible events, Γ is the probability of occurrence of a particular event *i* and *N* is the total number of objects that can undergo that event *i*. Once the total rate R is calculated, a random number is selected between 0 and R, which will determine which event will occur. In this manner, the event is selected randomly but with the appropriate weight according to its probability of occurrence. Once the event is picked, the simulation time is updated, increasing the time by a time increment, Δt, that is equal to the inverse of the total rate:

$$\Delta t = \frac{-\log \xi}{R} \quad (2)$$

Often, the time increment is multiplied by the logarithm of a random number, ξ, between 0 and 1, to ensure that a Poisson distribution of time is achieved.

After selecting the event, an object from all those that can realize that event is picked randomly. The actions associated to that event are then computed and the system is updated accordingly. For example, in the case we are interested in, radiation damage, an event could be the migration of a self-interstitial atom. The event in this case is the migration and the

object the self-interstitial. One self-interstitial is then selected randomly from all those existing in the system and displaced to a new location. In the case of an off-lattice kinetic Monte Carlo, the displacement is a fixed distance, usually taken between first and second nearest neighbours distance. Once the self-interstitial has been displaced, it is necessary to evaluate the new environment of that object and perform the necessary actions. For example, if the self-interstitial is located within the capture radius of another defect, the interaction and reaction between those defects must take place, therefore changing the defect distribution and configuration. One possibility in this example is that the self-interstitial moves to a location within the capture radius of a vacancy and consequently these two defects cancel each other, or that the self-interstitial moves within the capture radius of another self-interstitial and a di-interstitial must be created. Much of the simulation time is, in fact, spent in this part of the calculation. This also implies that every time step, the total rate must be recalculated since the number of objects for each event could, in principle, have changed. Figure 1 shows schematically the different steps in a general object kinetic Monte Carlo calculation.

The aforementioned algorithm is, however, not the only possible method for selecting events in a kinetic Monte Carlo. A different approach is used in the so-called Event kinetic Monte Carlo [23, 24] and first-passage kinetic Monte Carlo (FPKMC) [25]. Here, the time delay for all the possible events in the system is first calculated and the event selected is that with the shortest time delay. The event is then performed, taking care of all the associated changes, as explained above, and all the new time delays have to be calculated. The time in this case advances by the delay time of the event picked. This algorithm is used in codes such as JERK [24, 26] and has been used very successfully to compute the electrical resistivity of irradiated Fe [7] and Fe in the presence of impurities such as carbon [27]. In the EKMC method some approximations are made in order to calculate the delay time for events such as the interaction between two neighbouring objects. For more details on EKMC see references [24, 26-28].

A more general method has been developed by Opplestrup et al [25] named first-passage kinetic Monte Carlo (FPKMC). In this method, as in the EKMC algorithm, the event selected is the one that would occur in the shortest time from all possible events. However, FPKMC lacks the approximations included in EKMC. In FPKMC, each one of the walkers is surrounded by a “protective domain” and when a walker is selected it is moved to the edge of that domain. That results in a tremendous computational gain with respect to OKMC since many small jumps, that would have to be done in OKMC where the jump distance is fixed, are automatically avoided in FPKMC. However, the efficiency of FPKMC decreases significantly with respect to OKMC when the number of particles is high, since for each step, all the times associated to the jump of each walker to the edge of their “protective domains” have to be calculated. Some applications and comparisons between FPKMC and OKMC can be found in [29].

It is clear from the description above that the key parameters in KMC (either OKMC, EKMC or FPKMC) are the probabilities of the events in our system. Transition state theory (TST) can be used to obtain the rates between two different states [30]. For an extended description of TST and KMC see the review by A. Voter [31]. The transition rates are generally obtained from energy barriers between two different states of the system. Accurate models such as density functional theory (DFT) or others less precise, like calculations using empirical potentials, can be used to obtain these barriers. Details of these calculations can be found in section 1 of this special issue.

Once the activation energy is known, the rate for the event, Γ_i, is then obtained considering an Arrhenius dependence:

$$\Gamma_i = \Gamma_{i0} \exp\left(-E_a / KT\right) \qquad (3)$$

where Γ_{i0} is the jump or attempt frequency, E_a is the activation energy for that particular event, K is Boltzmann's constant and T is the temperature. As can be clearly seen from this description, the accuracy of the method depends on one hand, on the accuracy of the values of the different rates and, on the other hand, on the selected events and interactions to describe the system. How well this model reproduces the system we are interested in can only be assessed through extensive comparisons with experimental observations.

Table I gives a list of all the required parameters for a standard calculation of defect evolution in a material under irradiation, and the possible sources for these parameters. The objects in this case are the defects produced by the irradiation and the interactions between these defects and with the existing microstructure such as dislocations or grain boundaries. The starting point of the simulation is the distribution of the defects produced by the irradiation, including their location (x, y, z coordinates) and type (vacancy, self-interstitial, impurity). In the case of a continuous irradiation, new defects are introduced in the simulation box with a rate according to the dose rate of the experiment that is being simulated. As mentioned in the introduction, the positions and types of defects can be obtained from classical molecular dynamics simulations with empirical potentials (CMD), from binary collision approximation (BCA) calculations, such as those obtained from SRIM [32] or Marlow [33], or as a random distribution of Frenkel-pairs, depending on the type of experiment to be simulated. For example, when damage is produced by electrons the last approximation can be used. In the case of damage produced by light ions such as He, calculations using the binary collision approximation are appropriate. However, for self-irradiation and heavy-ions it is necessary to use those results obtained from molecular dynamics simulations. Often times a combination of BCA and MD calculations is used to obtain the distribution of defects during irradiation for energies that can not be reached by CMD alone. In this case the BCA is used to obtain the energies of those recoils produced by the energetic particle along its path, but the final defect distribution produced by those recoils is the one obtained from CMD simulations.

In some of the implementations of the OKMC algorithm, clusters are described by the location of its centre of mass, the number of defects and the type of defects in the cluster [15-21]. Codes such as Bigmac [34] or Lakimoca [18] use this approach. Each defect, either a single defect or a cluster, has associated a capture radius that depends on the number of defects of that object. This capture radius, r, is often defined as spherical:

$$r_n = \sqrt[3]{\frac{3n\Omega}{4\pi}} \qquad (4)$$

where n is the number of defects in the cluster and Ω is the atomic volume. This capture radius is used to define when two defects interact. Also when a defect dissolves from a cluster it is positioned outside this capture radius. When using this approach information regarding the lattice structure is lost. Strain effects such as the bias interaction between interstitials and dislocations can be included in this capture radius, increasing the capture

radius for interstitials. It is also possible to include strain effects in OKMC using elasticity theory [35, 36].

In other implementations of the OKMC, the location of all the defects in a cluster are kept in the simulation. This is in fact done in codes such as MMonCa [37] that has been used to model dopant diffusion in silicon [38] as well as metals [39-41]. This approach has the advantage that the location of defects in the cluster defines its capture volume and interactions with other defects can be defined more precisely. However, it is also computationally more expensive.

As mentioned above, in an OKMC for radiation damage, the objects are the defects produced during the irradiation, that is vacancies (V) and self-interstitials (I), but also impurities that could exist in the sample, such as carbon (C), or produced by transmutation in neutron irradiation or implanted, such as He. And the clusters that these defects can form among themselves must also be considered. One can see that in a system with 4 different types of objects (V, I, C and He, for example) the possible permutations between these different elements can give rise to a wide variety of complexes. From all these elements, the migration energy, dissociation of a defect from a cluster and the interaction between the different types of defects must be known. These are the possible events. For example the probability of a defect of type *t* undergoing a migration event is given by:

$$\Gamma_m^t = \Gamma_0^t \exp\left(-E_m^t / KT\right) \qquad (5)$$

where, as mentioned above, Γ^t_0 is the jump frequency, E^t_m is the migration energy for that particular type of defect, K is Boltzmann's constant and T is the temperature. Moreover, these objects can move in any direction (three-dimensional migration) or along a specific direction (one-dimensional migration) which is the case of some self-interstitial clusters in metals. When the object can migrate in any direction (three-dimensional migration) the jump is often performed by randomly placing the object within a sphere of radius the jump distance. When the migration of the object is restricted to one particular direction (one-dimensional migration), such as the case of some self-interstitial clusters in metals, a particular direction of motion (<111> for Fe and <110> for Cu, for example) with respect to the simulation box is given to the object when it is created, and the jumps are performed only along that direction.

Another basic type of event is the dissociation of a defect from a cluster. In this case, the probability of that defect dissociating from the cluster is given by:

$$\Gamma_d^t = \Gamma_0^t \exp\left(-\left(E_m^t + E_b^t\right) / KT\right) \qquad (6)$$

where E^t_b is the binding energy of the defect to the cluster. This energy depends on the number of defects in the cluster and the type of cluster.

Finally, all the possible interactions between defects must be taken into account. Here, the system can be made as simple or as complex as required by the particular objective of the simulation at hand. The simplest case could be considering only vacancies and self-interstitials and only one type of self-interstitial cluster. Then three reactions must be considered: $I_n + I_m \rightarrow I_{n+m}$ (self-interstitial cluster growth, where *n* and *m* are the number of

defects on each cluster), $V_n + V_m \rightarrow V_{n+m}$ (vacancy cluster growth) and I_n+V_m which could result in three different outcomes: annihilation of defects if n=m, a self-interstitial cluster of size n-m, I_{n-m}, if n > m, or a vacancy cluster of size m-n, V_{m-n}, if m>n. Nowadays, however, calculations of defect evolution in metals are much more complex, including the presence of impurities, such as C [40] or He [19, 42], different types of self-interstitial clusters [41] or even alloys [43]. Therefore, the list of possible reactions between defects can be very extensive. In such complex calculations one of the difficulties is to identify the relevant parameters that are the main drivers for microstructure evolution.

In the following sections we will describe some examples of OKMC calculations of microstructure evolution in irradiated metals under different conditions. These examples focus on the influence of the initial damage distribution, obtained from molecular dynamics simulations, on the microstructure that can be observed by techniques such as transmission electron microscopy.

3. Damage accumulation in pure metals: copper vs. iron

The first application of the OKMC method refers to damage evolution in two metals: copper, with an f.c.c. structure, and Fe with a b.c.c. lattice. The influence of the initial damage distribution in the microstructure evolution is clearly observed when comparing damage accumulation in these two metals. Molecular dynamics simulations of recoils with the same energy in these two materials show that, although the total number of defects produced is very similar, the defect distribution is quite different. For 30keV cascades, such as those shown in figure 2 as a representative example, in copper almost every single cascade will produce a vacancy cluster at the initial location of the PKA surrounded by self-interstitial clusters, normally of smaller size than the vacancy one as shown in figure 2(a) where green spheres represent the location of vacant sites and red ones are self-interstitials. These vacancy clusters evolve into stacking fault tetrahedra over longer periods of time, as shown by other authors [44]. The size of these vacancy clusters is of the order of 1.5 nm in radius. On the other hand, in iron, the damage produced for the same recoil energy consists mostly of isolated vacancies, also located mostly near the center of the collision cascade, surrounded by self-interstitial clusters, as shown in the example in figure 2(b). Self-interstitial clusters are usually smaller in the case of Fe than in Cu. These cascades were calculated using embedded atom type of potentials, [45] and [46] for copper and iron respectively.

In Ref. 16, using a database of collision cascades as initial defect distribution, the accumulation of damage and microstructure evolution with time was studied with OKMC for these two materials. In this case 20 keV cascades were used. The calculations were performed for the same homologous temperature, 0.25 of the melting point (340K and 363K for Cu and Fe respectively) using the OKMC code BIGMAC, developed at LLNL [34].

The migration and binding energies for Cu vacancies were taken from calculations by Sabochick et al. [47, 48] while for self-interstitials the values of Schober and Zeller were used [49]. For iron, on the other hand, values for vacancies and self-intersitials were calculated by Diaz de la Rubia and Soneda and used in these calculations [50]. Note that at the time, the state-of-the-art interatomic potentials for Fe predicted the <111> self-interstitial as the most stable one, with almost athermal migration (E_m ~ 0.1 eV) just like in the case of copper. Since then, DFT calculations have reviled that the most stable configuration for the self-interstitial in Fe is the <110> dumbbell with a higher migration barrier (Em ~ 0.3 eV [51]). It was in fact through a combination of DFT calculations and a kinetic Monte Carlo model, in this case an

Event Kinetic Monte Carlo, briefly described above, that it was possible to interpret the experimental measurements of resistivity recovery of electron irradiated Fe, showing that indeed, it is the <110> dumbbell the most stable, as well as the formation of other defects [7]. Nevertheless, as an example of OKMC calculations and for the sake of comparison between these two materials, particularly regarding the effect of initial defect distribution, the results first published in 2000 are still valid [16].

In the case of copper, self-interstitial clusters of sizes smaller than 60 defects were considered mobile and if they traveled a distance equivalent to 1 micron, they were removed from the simulation box, effectively considering a grain boundary size of 1 micron. In Fe, self-interstitial clusters are also mobile but when they were within the capture radius of each other they form a junction and become immobile.

Damage accumulation at a dose rate of 10^{-4} dpa/s for both metals was calculated. In iron, 5 atomic parts per million (appm) of interstitial impurity atoms were included in the simulation, which act as perfect traps for self-interstitial atoms and small self-interstitial clusters.

Figure 3(a) shows the total cluster concentration as a function of irradiation dose for the two metals, copper (in red) and iron (in blue). Note that the total concentration is very similar for both metals. However, experimentally it is well known that the cluster concentration measured with TEM in these materials is at least one order of magnitude lower in iron than in copper [52]. If we analyze these results in more detail we can see that in copper most self-interstitials and self-interstitial clusters disappear through recombination with vacancies or at grain boundaries, and most of the damage is formed by vacancy clusters. This is significantly different in the case of iron where both self-interstitial and vacancy clusters are present. However, the size of these clusters are very different between the two materials, in copper vacancy clusters with up to 30 defects are observed, as a consequence of the clustering occurring in the collision cascade, while in iron the largest vacancy clusters have less than 15 defects. Self-interstitial clusters in iron are larger with sizes with up to 60 defects in a cluster.

The comparison with TEM measured defect densities can only be done considering the threshold for visibility in these experiments. Using a threshold of 20 defects for vacancies in copper, equivalent to a stacking-fault tetrahedra of ~1.5 nm, 350 vacancies for a 1nm void in Fe and 50 self-interstitials for a 1 nm loop in Fe, we obtain the results of the visible cluster concentration as a function of dose in copper and iron shown in figure 3 (b). Here, the one order of magnitude difference between copper and iron observed experimentally is clearly reviled.

The results for copper and their dependence with the different parameters in the OKMC model are clear. Moreover, the cluster concentration obtained matched remarkably well the experimental measurements as shown in [16]. Besides the cluster concentration, the average number of vacancies in a cluster are also in agreement with experiment, ~28 (~2 nm) and constant with dose, showing that these defects are formed directly in the collision cascade. Therefore, for copper, the two most relevant parameters that can explain the experimental observations are (1) formation of vacancy clusters within the few picoseconds time frame of the collision cascade (2) fast migration of self-interstitial clusters. For the case of iron, however, the correlation between simulations and experiments is not so straightforward. On one hand, the lack of significant clustering within the collision cascade implies that most of the evolution of the clusters and growth to sizes that can be observed

experimentally is going to occur through defect diffusion and defect coalescence. And the description of these interactions depends completely on the set of reactions that the user of the OKMC model has decided to consider as the important ones. That is, there is not an unambiguous description of defect evolution in Fe which is, in fact, the reason for much of the controversy in the modeling of microstructure evolution of this material. This discussion, however, is beyond the scope of this review paper.

4. Void swelling in f.c.c. and b.c.c. materials

The influence of initial damage structure on void swelling was also studied with an OKMC model [42, 53]. Void swelling is a phenomena observed mostly in austenitic steels while ferritic steels seem to be more resistant to it [54]. This effect is due to, on one hand, the stabilization of vacancy clusters by the presence of impurities, mostly helium, and the fast migration of self-interstitials to sinks [55]. Therefore, in this case, it is necessary to include in the OKMC model all the reactions between vacancies and self-interstitials with helium. This results in a matrix that can expand really quickly since both the number of helium and the number of vacancies in the cluster will increase as a mixed He-vacancy cluster. Therefore, the values for the binding energies of defects to clusters of type He_nV_m, where n is the number of helium atoms in the cluster and m is the number of vacant sites, must be obtained from some model, either from static calculations with empirical potentials or from first principles density functional theory. The usual procedure in this case is to compute the binding energies of a few representative but small clusters using DFT and then use an interatomic potential that has been validated with these results, to obtain the values for larger clusters. In this example, the values for binding energies calculated by Adams and Wolfer [56] were used. These were calculated using empirical potentials. In the calculations these values are kept the same for all simulations and only the source term, that is, the initial distribution of defects, is changed, using defect distributions from iron and copper cascades, similar to the example in the previous section.

Calculations are performed for the same total dose (0.1 dpa) and for different temperatures. For each cascade a Helium atom is introduced in the simulation, or a total of 1000 appm of He per dpa. The number of vacancies in clusters containing He are counted as those contributing to swelling. From this number and assuming a relaxation volume for a vacancy in He_nV_m cluster to be 0.8 Ω atomic volume we obtain the equivalent of a % of swelling. Figure 4 shows the results obtained for the % of swelling as a function of temperature for the same total dose and for two different initial configurations of the cascade damage. We observe that when clusters are present in the collision cascade, a swelling dependence with temperature very similar to that measured experimentally for f.c.c. materials [54], with a clear swelling peak. Note that not only vacancy clustering is necessary to produce swelling. Vacancy clustering is needed as the seed to nucleate He_nV_m clusters, however, in order to have swelling an efficient removal of self-interstitials is required, which in this case occurs due to the clustering of self-interstitials and their fast migration to sinks such as dislocations or grain boundaries. These are, in fact, the main components of the ‘production bias’ model described by Woo and Sing [55] and based on the early results of molecular dynamics simulations of collision cascades in metals.

In the case of cascade damage with small self-interstitial clusters and dispersed, isolated vacancies, calculations show that swelling is very small (blue line in figure 4) in comparison with the case described above where defects were mainly in clusters. This comparison is done for the same total dose measured in dpa (displacements per atom), that is, for the

same number of defects produced in the irradiation. The green curve in this case includes not only the vacancies in He_nV_m but also those in vacancy clusters without He, although no significant differences are observed. Swelling only increases slightly with temperature in this case, reproducing those results observed in b.c.c. materials such as iron [54]. The reason for this difference is that now vacancies must first migrate and form clusters that serve as the nuclei for He_nV_m bubbles or voids. But many of these vacancies will recombine with the nearby self-interstitial clusters which, even though they can also migrate, they are smaller than in the case of copper, therefore more disperse increasing the probability of recombination with vacancies. These vacancies can also diffuse to other sinks such as grain boundaries or dislocations. In brief, the higher recombination between vacancies and self-interstitials in a disperse collision cascade results in lower densities of nuclei for bubbles and voids and consequently lower swelling. As mentioned above, these results can only be qualitatively compared to experiments mainly due to the low doses reached in the calculations compared to the existing measurements, as well as the lack of accurate enough parameters for He_nV_m clusters. Despite the limitations, these simulations show that some of the features observed in the microstructure evolution of irradiated materials are directly related to defect distributions produced in the core of a collision cascade. And this link between the picosecond time frame of molecular dynamics simulations and experimental observations can only be performed through the use of an OKMC model.

5. Influence of the interatomic potential on collision cascades and microstructure evolution: the case of Fe

The two cases described above involved a comparison between materials where the defect damage distribution originated in the collision cascade is quite different in terms of clustering of vacancies and self-interstitials. One question emerges regarding the influence of the interatomic potential selected for the calculation of the collision cascade on the later evolution of the damage. Up to now, the results obtained from molecular dynamics on defect distribution in the picosecond time frame can not be directly validated experimentally. Only, as explained above, the evolution of this damage with the use of OKMC can be compared to experiments. However, many other factors are then present in these simulations: migration energies, binding energies, reactions between defects or defect capture radius among others. On the other hand, it is well known that for the same material, recoil energy and temperature, different interatomic potentials will result in different clustering fractions of defects [57, 58], even though the total number of Frenkel pairs produced will be very similar. This raises the question of how these differences will affect the long term damage evolution. Are those differences significant enough to give rise to a difference on the long term evolution of the microstructure? In order to answer this question we performed OKMC calculations where all parameters regarding migration energies, binding energies, defect interactions and capture radius were kept the same and the only difference between the calculations were the database of cascades used, calculated for Fe with three different interatomic potentials and for the same energy (50 keV) and recoil conditions [59]. The database of cascades used in these calculations were obtained with the following interatomic potentials: the one developed by Ackland, Mendelev and Srolovitz (AMS) [60], the one from Dudarev and Derlet with short range potential fit by Björkas and Nordlund (DD-BN) [61] and one developed by Müller, Erhart, and Albe with short range part by Björkas and Nordlund (MEA-BN) [62]. All three potentials produce, on average, very similar number of Frenkel-pairs, however, the AMS potential gives rise to large self-interstitial clusters (more than 100 defects) that do not appear in the other two potentials within the statistics of these calculations. For more details see ref. [59]. Although the number of large self-interstitial

clusters is small, it is interesting to see how the presence of these clusters affects the subsequent damage evolution.

Figure 5(a) shows the total number of clusters as a function of dose obtained for all three potentials and the same conditions of irradiation (dose rate, temperature, concentration of traps, etc.) showing no significant difference. However, when only visible clusters are considered, that is, clusters with more than 55 defects, then the difference in damage accumulation between the three potentials is clearly observed, as shown in figure 5(b). The potential with the largest self-interstitial clusters formed in the collision cascade (AMS) has a smaller slope for defect growth with dose but visible clusters appear at a lower dose than in the case of the other two potentials that show a steeper slope.

These results show, firstly, the importance of the initial defect distribution on damage evolution. Even if the probability of having large self-interstitial clusters is small, their presence determines how the damage is going to grow under subsequent cascades and over long periods of time. On the other hand, these results also provide a possible path for validating interatomic potentials in terms of the cluster size distribution obtained in the collision cascade. Experimentally, the slopes that are measured for cluster concentration as a function of dose depends on the type of ion irradiation. In Fe, heavy ions give rise to a slope close to 1, since large self-interstitial clusters are formed and therefore they can easily grow to visible sizes, while irradiation with Fe ions results in higher slopes, ~2, meaning self-interstitial clusters formed in the collision cascade are smaller and in order to become visible coalescence between clusters as well as cluster growth due to diffusion of small self-interstitial clusters or mono-interstitials is required to reach sizes visible under TEM. However, experimentally slopes as large as 4 have not been observed. This means that some type of clustering must occur within the collision cascade and that the MEA interatomic potential is not able to capture this behavior.

It is important to point out that the validation of the interatomic potential in this manner is not straight forward. As mentioned earlier, many other parameters are involved when looking at microstructure evolution. This is particularly important in the case of Fe where clustering in the collision cascade is generally small compared to other materials like W (see ref. [63]) or Cu (see figure 2(a)). Therefore, in Fe the coalescence of self-interstitial clusters and growth beyond the collision cascade phase is needed to reach those sizes observed experimentally. And these processes are governed by the reactions between loops and defects mobilities selected in the OKMC model. This approach could, in fact, be more successful in other materials where clustering in the collision cascade is larger, and the subsequent interaction among defects in the cascade does not play such as significant role as in Fe, like in the case of copper mentioned in section 3 above, or tungsten for b.c.c. materials.

6. Beyond the standard OKMC models

Currently there is a wide interest on enhancing the capabilities and accuracy of kinetic Monte Carlo models. On one hand, there is a considerable effort devoted to improve the efficiency of this method so that longer times and larger system sizes can be modelled. Nowadays, with the existence of supercomputers, parallelization would seem an obvious way to improve performance of these calculations. Parallelization is relatively simple in an EKMC or FPKMC algorithm. However, in the OKMC algorithm the total rate for all events in the system must be computed at each time step. This means that all nodes must know of all events at every time step, therefore making the parallelization very inefficient. Recently,

Martinez et al. [64] have developed a synchronous parallel algorithm that, unlike previous attempts, solves the same master equation as the serial algorithm. In this case, the total rate of all events on each processor is kept fixed for all processors by including null events. A different approach has been developed by Jimenez and Ortiz [65] making use of GPUs for the parallelization of the OKMC algorithm.

Another aspect in the improvement of the OKMC method is trying to find a way to avoid the arbitrary selection of the events that go into the calculation. One of the great advancements in this area is what is known as on-the-fly kinetic Monte Carlo. The basic idea of this method is to compute the rates of the specific processes at the same time as the kinetic algorithm is evolving. That is, the event rates are not tabulated before the KMC calculation starts. This is particularly important for those systems where the different type of events are very large and it is not possible, a priori, to know or define every scenario. This is, for example, the case of defect diffusion in alloys, in particular, in concentrated alloys, where the rate of a particular reaction will depend on the local environment. The methodologies used to implement an on-the-fly KMC algorithm differ between different groups and is adapted to the type of problem that needs to be solved. Probably the first on-the-fly KMC model is the one by Henkelman and Jónsson [66]. The authors use the dimer method [67] to obtain the saddle points between different states and construct an event catalogue. Stress-assisted diffusion of hydrogen in iron has been studied [68] combining on-the-fly calculations of barriers using empirical potentials with pre-calculated barriers with more accurate density functional theory. For other examples of on-the-fly KMC see references [69-72]. One promising on-the-fly method is the one developed by Xu et al [73] called self-evolving atomistic kinetic Monte Carlo (SEAKMC). In this case, longer simulation times can be achieved by defining “active volumes” around the defect of interest [74, 75]. For the case of defect evolution in alloys other specific methods have been developed to produce the catalogue of transition rates in a more efficient way. One of those methods consists of using artificial neural networks to predict the values of the energy barriers [76]. Another method makes use of the phase diagram to bias defect diffusion and considers the local concentration to calculate the defect rates [77].

There are still challenges in the field of object kinetic Monte Carlo. Avoiding the *ad hoc* selection of the processes to include in the calculations still remains an open question. And probably one of the missing important components is taking into account in a general form the elastic field interactions between defects, although some important advances are being achieved as in the work of Mason et. al [78].

7. Conclusions

In this review, after introducing the methodology behind object kinetic Monte Carlo, we have shown how this algorithm can be used to study microstructure evolution of irradiated materials. The OKMC method provides a connection between atomistic simulations of migration energies, binding energies or defect distributions with experimentally meaningful time and length scales, and therefore a way of validating these parameters or evaluating their influence on microstructure evolution. In this respect, we have shown three examples of how the picosecond time defect distribution, obtained from molecular dynamics simulations of collision cascades, has an important impact on the microstructure evolution.

However, care must be taken when drawing conclusions from OKMC calculations as those described here. In all these simulations there is always a selection from the part of the user

of the reactions and mechanisms included in the calculations. A model will only be robust if, with the same input parameters regarding defect migration, binding energies and interactions, is able to reproduce different experimental conditions. Further improvements of the OKMC algorithm to avoid this *ad hoc* selection of reactions would be desirable. In this respect, there are many efforts towards a more first principles based type of algorithm such as the SEAKMC model developed at Oak Ridge National Laboratory [73-75] or those being developed at CCFE [78]. These models, however, are much more costly. If a connection to experiments at high doses (several dpa) has to be established, then it is necessary to make use of the OKMC approach described here with selected reactions. And these advanced tools can help in the selection of the proper parameters and interactions.

Acknowledgments

I would like to thank my co-authors in the works briefly described here. This work has been carried out within the framework of the EUROfusion Consortium and has received funding from the Euratom research and training programme 2014-2018 under grant agreement No 633053. The views and opinions expressed herein do not necessarily reflect those of the European Commission. The research leading to these results is partly funded by the European Atomic Energy Community's (Euratom) H2020 WP 2016-2017 call NFRP13 (M4F) and in the framework of the EERA (European Energy Research Alliance) Joint Programme on Nuclear Materials.

Data Availabilty

The raw/processed data required to reproduce these findings cannot be shared at this time since this is a review article.

References

[1] E. Chason, S.T. Picraux, J.M. Poate, J.O. Borland, M.I. Current, T.D. de la Rubia, D.J. Eaglesham, O.W. Holland, M.E. Law, C.W. Magee, J.W. Mayer, J. Melngailis, A.F. Tasch, J. Appl. Phys. 81 (1997) 6513.

[2] S. J. Zinkle, J. T. Busby, Materials Today 12 (2009) 12-19

[3] J. Knaster, A. Moeslang, T. Muroga, Nature Physics 12 (2016) 424-434

[4] A. A. Tseng, Small 1 (2005) 924-939

[5] A. Stanishevsky, B. Nagaraj, J. Melngailis, R. Ramesh, L. Khriachtchev, E. McDaniel, J. of Appl. Phys. 92 (2002) 3275-3278

[6] R. Phillips, Cristals, Defects and Microstructures, Mode.ing Across Scales, Cambridge University Press, Cambridge, (2001)

[7] C.-C. Fu, J. Dalla-Torre, F. Willaime, J.-L. Bocquet, A. Barbu, Nature Materials **4** (2005) 68

[8] D. P. Kroese, T. Brereton, T. Taimre, Z. I. Botev, WIREs Computational Statistics, 6 (2014) 386-392

[9] N. Metropolis and S. Ulam, Journal of the American Statistical Association 44 (1949) 335-341.

[10] N. Metropolis, Los Alamos Science, Special Issue (1987) 125-130

[11] R. Eckhardt, Los Alamos Science, Special Issue (1987) 131-141

[12] J.R. Beeler, Jr., Phys. Rev. 150 (1966) 470

[13] D. G. Besco, Computer Simulation of Point Defect Annealing in Metals, USA-AEC Report GEMP-644, October 1967.

[14] D. G. Doran, Radiat. Eff. 2 (1970) 249.

[15] H. L. Heinisch, H.L. Radiat. Eff. Def. Solids 113 (1990) 53.

[16] M.J. Caturla, N. Soneda, E. Alonso, B.D. Wirth, T. Díaz de la Rubia, J.M. Perlado, J. Nucl. Mater. **276** (2000) 1

[17] C. Domain, C.S. Becquart, L. Malerba, J. Nucl. Mater. **335** (2004) 121.

[18] V. Jansson, M. Chiapetto, L. Malerba, J. of Nucl. Mater. 442 (2013) 341-349

[19] K. Morishita, R. Sugano, Nucl. Instru. And Meth. B 255 (2007) 52-56

[20] C. S. Becquart, M. F. Barthe, A. De Backer, Physica Scripta T145 (2011) 14048

[21] J. Marian, C. S. Becquart, D. Domain, S. L. Dudarev, M. R. Gilbert, R. J. Kurtz, D. R. Mason, K. Nordlund, A. E. Sand, L. L. Snead, T. Suzudo, B. D. Wirth, Nucl. Fusion 57 (2017) 92008

[22] M. H. Kalos, Monte Carlo Methods, vol. I, Basics. John Wiley & Sons, 1986

[23] J.-M. Lanore, Rad. Eff. 22 (1974) 153-162

[24] J. Dalla Torre, J-L. Bocquet, N.V. Doan E. Adam, A. Barbu, Phil. Mag. **85** (2005) 549.

[25] T. Opplestrup, V. Bulatov, G.H. Gilmer, M.H. Kalos, B. Sadigh, Phys. Rev. Lett. **97** (2006) 230602

[26] J. Dalla Torre, C. C. Fu, F.Willaime, A. Barbu, and J.-L. Bocquet, J. Nucl. Mater. 352, 42 (2006)

[27] T. Jourdan, J.-P. Crocombette, Phys. Rev. B 86 (2012) 54113

[28] C. S. Becquart, A. Barbu, J. L. Bocquet, M. J. Caturla, C. Domain, C-C. Fu, S. I. Golubov, M. Hou, L. Malerba, C. J. Ortiz, A. Souidi, R. E. Stoller, J. Nucl. Mater. **406** (2010) 39.

[29] A. Donev, V. Bulatov, T. Opplestrup, G.H. Gilmer, B. Sadigh, M. H. Kalos, J. of Computational Physics 229 (2010) 3214

[30] R. Marcelin, Ann. Physique 3 (1915) 120

[31] A. F. Voter, Radiation effects in Solids, 235 (2007) 1-23

[32] J. F. Ziegler, J. Biersack, U. Littmark, *The Stopping and Range of Ions in Matter* (1985) Pergamon Press

[33] M. T. Robinson, Phys. Rev. B 67 (1992) 396-400

[34] M. Johnson, M. J. Caturla, T. Diaz de la Rubia, J. of Applied Physics **84** (1998) 1963

[35] L. Z. Sun, N. M. Ghoniem, S. H. Tong, B. N. Singh, J. Nucl. Mater. **283-287** (2000) 741

[36] T. Hudson, S. L. Dudarev, M. J. Caturla, A. P. Sutton, Phil. Mag. **85** (2005) 661

[37] I. Martin-Bragadop, A. Rivera, G. Valles, J. L. Gomez-Selles, M. J. Caturla, Computer Physics Comm. 184 (2013) 2703

[38] I. Martin-Bragado, R. Borges, J. P. Balbuena, M. Jaraiz, Progress in Mat. Sci. 92 (2018) 1-32

[39] G. Valles, I. Martin-Bragado, K. Nordlund, A. Lasa, C. Björkas, E. Safi, J. M. Perlado, A. Rivera, J. of Nucl. Mat. 490 (2017) 108-114

[40] D. Terentyev, I. Martin-Bragado, Scripta Materialia 97 (2015) 5-8

[41] M. J. Aliaga, I. Dopico, I. Martin-Bragado, M. J. Caturla, Phys. Status Solidi A 213 (2016) 2969-2973

[42] M. J. Caturla, T. Diaz de la Rubia, M. Fluss, J. of Nucl. Mat. 323 (2003) 163-168

[43] M. Chiapetto, C. S. Becquart, L. Malerba, Nuclear Materials and Energy 9 (2016) 565-570

[44] B. Uberuaga, R. G. Hoagland, A. F. Voter, S. M. Valone, Phys. Rev. Lett. 99 (2007) 135501

[45] S.M. Foiles, M.I. Baskes, M.S. Daw, Phys. Rev. B 33 (1986) 7983

[46] R.A. Johnson, D.J. Oh, J. Mater. Res. 4 (1989) 1195

[47] M.J. Sabochick, S. Yip, N.Q. Lam, J. Phys. F 18 (1988) 349

[48] M.J. Sabochick, S. Yip, N.Q. Lam, J. Phys. F 18 (1988) 1689

[49] H.R. Schober, R. Zeller, J. Nucl. Mater. 69&70 (1978) 176.

[50] N. Soneda, T. Diaz de la Rubia, Philos. Mag. A 78 (1998) 995

[51] C. Domain, C. S. Becquart, Phys. Rev. B 65 (2001) 024103

[52] Y. Dai, M. Victoria, Mater. Res. Soc. Symp. Proc. 439 (1997) 319

[53] M. J. Caturla, N. Soneda, T. Diaz de la Rubia M. Fluss, J. Nucl. Mat. 351 (2006) 78

[54] B.N. Singh, S.J. Zinkle, J. Nucl. Mater. 206 (1993) 212

[55] C.H. Woo, B.N. Singh, Philos. Mag. A 65 (1992) 889

[56] J.B. Adams, W.G. Wolfer, J. Nucl. Mater. 166 (1989) 235

[57] C. Björkas and K. Nordlund, Nucl. Instrum. Meth. Phys. Res., Sect. B 259, 853 (2007)

[58] D. Terentyev, C. Lagerstedt, P. Olsson, K. Nordlund, J. Wallenius, C. S. Becquart, L. Malerba, J. of Nucl. Mat. 351 (2006) 65-77

[59] C. Björkas, K. Nordlund, M. J. Caturla, Phys. Rev. B 85 (2012) 024105

[60] G. J. Ackland, M. I. Mendelev, D. J. Srolovitz, S. Han, and A. V. Barashev, J. Phys. Condens. Matter 16, S2629 (2004)

[61] S. L. Dudarev and P. M. Derlet, J. Phys. Condens. Matter 17, 1 (2005)

[62] M. Müller, P. Erhart, and K. Albe, J. Phys. Condens. Matter 19, 326220 (2007)

[63] A. Sand, S. L. Dudarev, K. Nordlund, EPL 103 (2013) 46003

[64] E. Martinez, J. Marian, M. H. Kalos, J. M. Perlado, Journal of Computational Physics 227 (2008) 3804–3823

[65] F. Jimenez, C. J. Ortiz, Computational Materials Science, 113 (2016) 178

[66] G. Henkelman, H. Jonsson, J. of Chem. Phys. 115 (2001) 9657

[67] G. Henkelman and H. Jonsson, J. Chem. Phys. 111 (1999) 7010

[68] A. Ramasubramaniam, M. Itakura, M. Ortiz, E. A. Carter, J. of Materials Research 23 (2008) 2757

[69] S. Blackwell, R. Smith, S. D. Kenny, J. M. Walls, C. F. Sanz-Navarro, J. of Physics-Condensed Matter 25 (2013) 135002

[70] M. Robinson, S. D. Kenny, R. Smith, M. T. Storr, J. of Nucl. Mat. 423 (2012) 16

[71] L. Vernon, S. D. Kenny, R. Smith, E. Sanville, Phys. Rev. B 83 (2011) 075412

[72] Ell-Mellouhi, N. Mousseau, L. J. Lewis, Phys. Rev. B 78 (2008) 153202

[73] H. Xu, Yu. N. Osetsky, R. E. Stoller, Phys. Rev. B **84** (2011) 132103.

[74] H. Xu, Yu. N. Osetsky, R. E. Stoller, J. Phys.: Condens. Matter 24 (2012) 375402.

[75] H. Xu, Yu. R. E. Stoller, L. K. Béland, Y. N. Osetsky, Comp. Mat. Science 100 (2015) 135

[76] N. Castin, L. Malerba, J. Chem. Phys. 132 (2010) 074507

[77] I. Dopico, P. Castrillo, I. Martin-Bragado, Acta Materialia 95 (2015) 324

[78] D R Mason, X Yi, M A Kirk, S L Dudarev, J. of Physics: Condensed Matter, 26, (2014) 375701

Tables:

Table I: Description of required input parameters for a standard calculation of defect evolution in an irradiated material and possible methods and sources to obtain this input.

Input parameters required	**Possible sources/methods**
Initial defect distribution	CMD, BCA, random distribution
Capture radius	CMD, DFT, Elasticity theory
Migration energies	CMD, DFT
Dissociation energies	CMD, DFT, Elasticity theory
Defect-defect interactions	CDM, DFT, Elasticity theory

Figure captions:

Figure 1: Schematic representation of an object kinetic Monte Carlo algorithm.

Figure 2: Representative cascade damage produced by 30 keV recoil atoms in (a) copper and (b) iron. Green spheres represent the location of the vacant sites while red ones are the location of self-interstitials.

Figure 3: (a) Total cluster concentration as a function of dose for copper and iron (b) visible cluster concentration.

Figure 4: Void swelling as calculated from the OKMC model as a function of temperature for two different initial damage distributions, one with clusters as in an f.c.c. material such as copper (red line) and one with mostly small clusters or isolated monovacancies and mono-interstitials, like in the case of iron (blue and green curves). In the green curve, both the vacancies in clusters containing He and those without are counted to obtained the void swelling.

Figure 5: Cluster concentration in irradiated iron as a function of dose for calculations with initial configurations of defects obtained with three different interatomic potentials (a) Total cluster concentration (b) Visible cluster concentration.

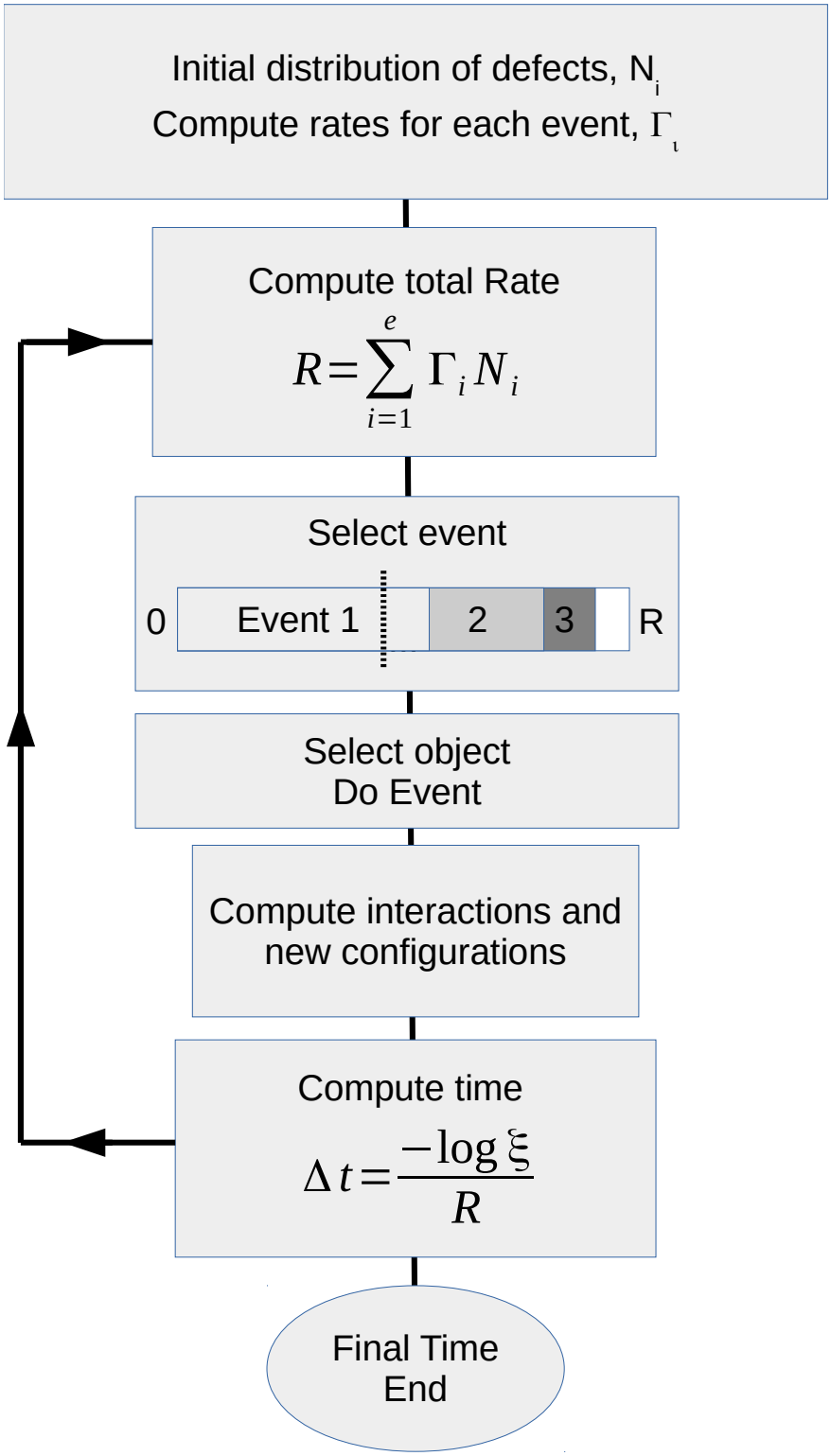
Initial distribution of defects, N_i
Compute rates for each event, Γ_i
Compute total Rate
$R=\sum_{i=1}^{e}\Gamma_i N_i$
Select event
0
Event 1
2
3
R
Select object
Do Event
Compute interactions and new configurations
Compute time
$\Delta t=\frac{-\log \xi}{R}$
Final Time
End

Figure 1

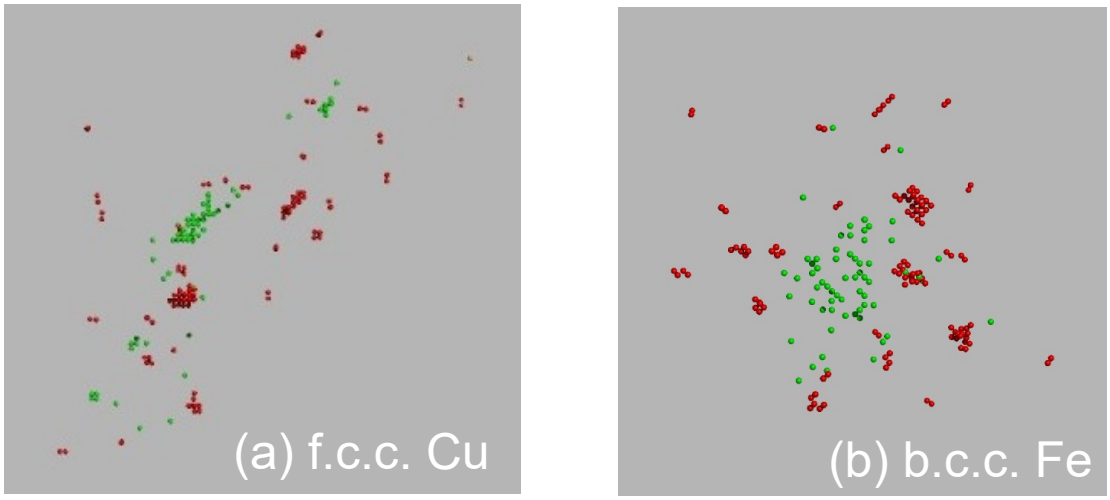

Figure 2

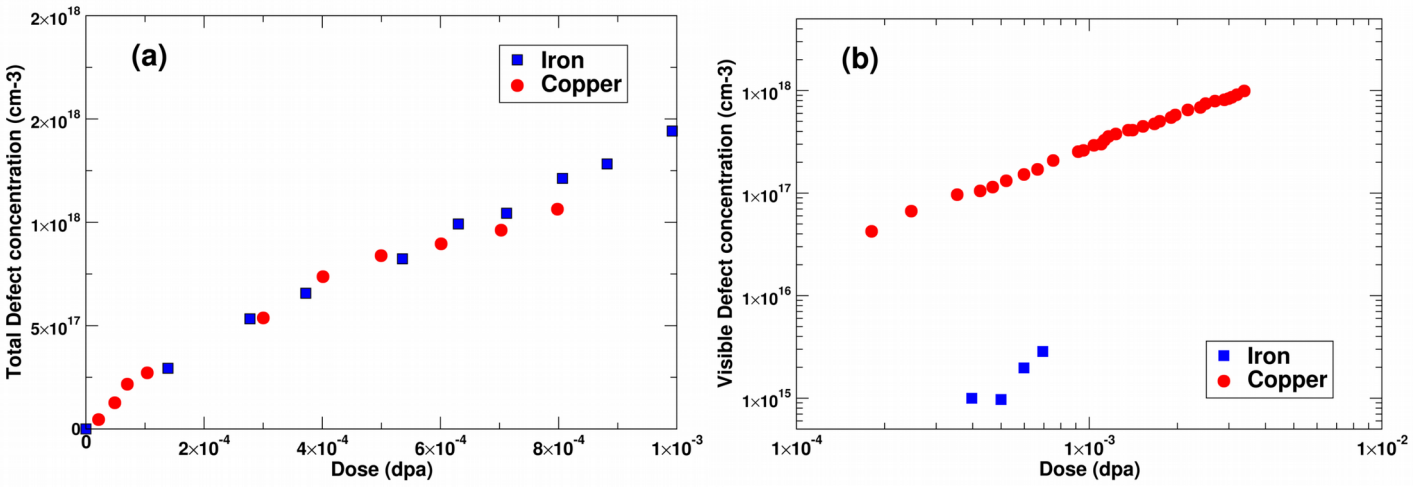
(a)
Iron
Copper
Total Defect concentration (cm-3)
Dose (dpa)
(b)
Iron
Copper
Visible Defect concentration (cm-3)
Dose (dpa)

Figure 3

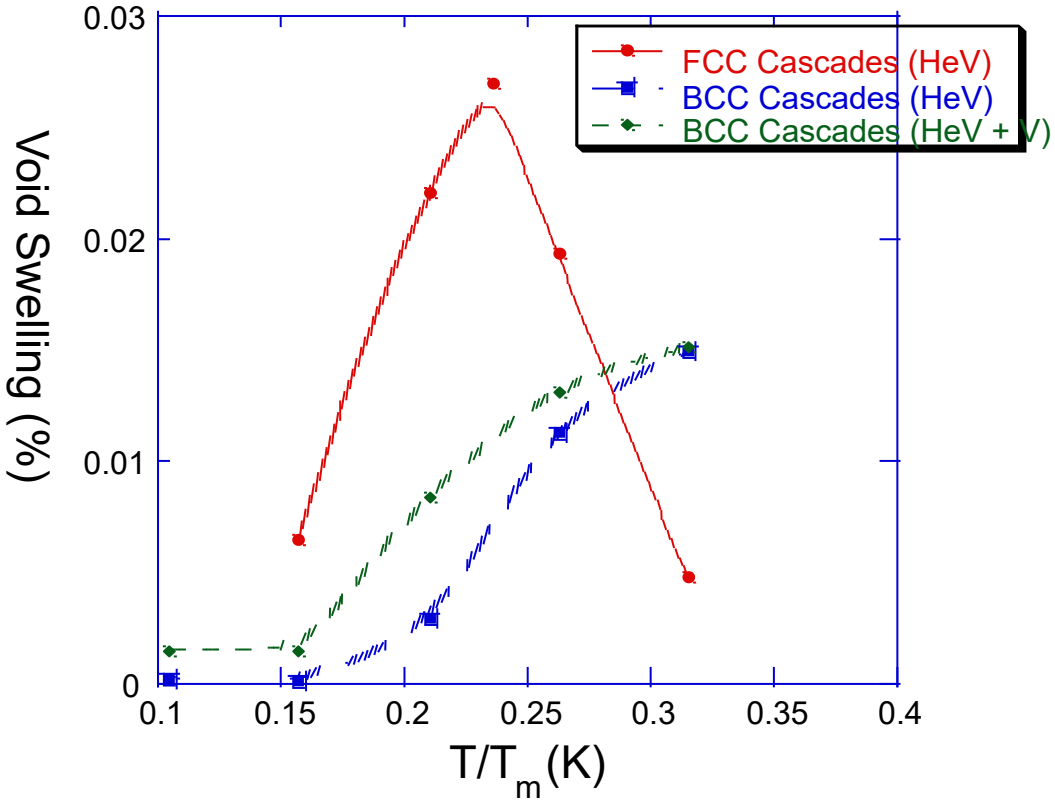
0.03
0.02
0.01
0
Void Swelling (%)
0.1
0.15
0.2
0.25
0.3
0.35
0.4
T/T_m (K)
FCC Cascades (HeV)
BCC Cascades (HeV)
BCC Cascades (HeV + V)

Figure 4

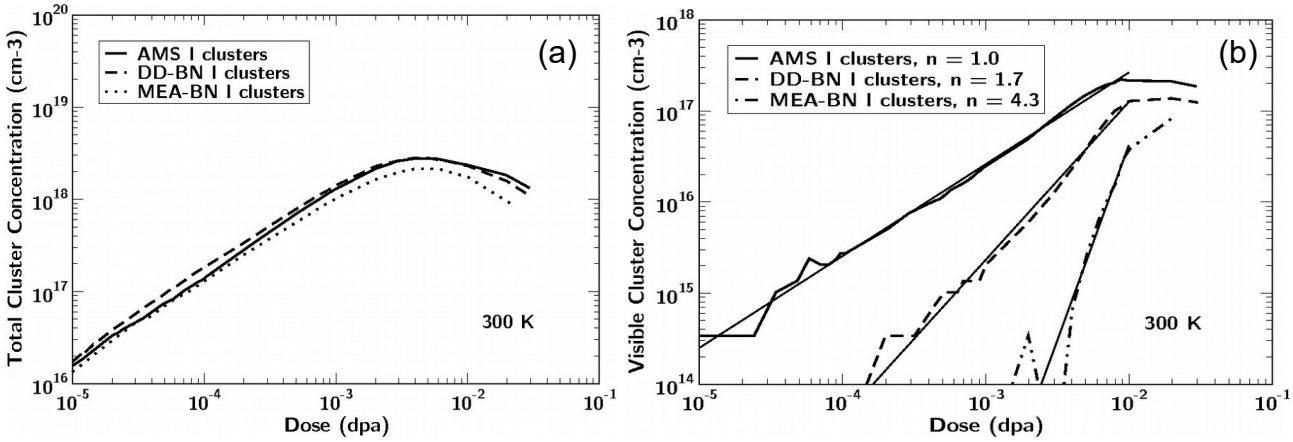
AMS I clusters
DD-BN I clusters
MEA-BN I clusters
(a)
300 K
Total Cluster Concentration (cm-3)
Dose (dpa)
AMS I clusters, n = 1.0
DD-BN I clusters, n = 1.7
MEA-BN I clusters, n = 4.3
(b)
300 K
Visible Cluster Concentration (cm-3)
Dose (dpa)

Figure 5